NeuroImage: Clinical 50 (2026) 103981

Contents lists available at ScienceDirect

NeuroImage: Clinical

journal homepage: www.elsevier.com/locate/ynicl

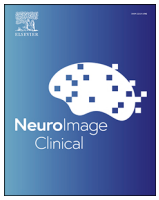

Functional gradient analysis reveals potential therapeutic mechanisms of nrTMS for postoperative motor deficits in glioma patients: A randomized controlled trial

Yuzhe Li [a,b,d], Jiangwei Wang [c], Zhong Zhang [b], Xing Fan [c], Yinyan Wang [b], Wenbin Ma [a,d,*], Tao Jiang [b,c,d,*], Shengyu Fang [b,*]

[a] Chinese Academy of Medical Sciences and Peking Union Medical College, Beijing 100037, China
[b] Department of Neurosurgery, Beijing Tiantan Hospital, Capital Medical University, Beijing, China
[c] Beijing Neurosurgical Institute, Capital Medical University, Beijing, China
[d] Research Unit of Accurate Diagnosis, Treatment, and Translational Medicine of Brain Tumors, Chinese Academy of Medical Sciences, Beijing, China

ARTICLE INFO

Keywords:
Glioma
nrTMS
Functional gradients
Motor deficit

ABSTRACT

Objective: This study aimed to investigate the therapeutic effects and neural mechanisms of high-frequency neuro-navigated repetitive transcranial magnetic stimulation (nrTMS) targeting the hand knob in glioma patients with postoperative motor deficits, using functional gradient analysis to characterize cortical reorganization.

Methods: Thirty patients with postoperative motor deficits were randomized to receive nrTMS or sham stimulation targeting the ipsilateral hand knob. Motor function was assessed using Fugl-Meyer Assessment (FMA) and muscle strength. Resting-state fMRI was acquired to compute principal functional gradients. Control/tumor, nrTMS/sham, and Pre-TMS/Post-TMS gradient changes were analyzed. Correlation and regression analyses related to motor recovery were performed.

Results: The nrTMS group showed significantly greater improvement in muscle strength (Post-treatment: nrTMS: 3.533 ± 0.720, Sham: 2.067 ± 0.572, $p = 0.019$, $d = 1.082$; 3-month follow-up: nrTMS: 4.600 ± 0.408, Sham: 3.733 ± 0.609, $p = 0.035$, $d = 1.012$). Gradient analysis revealed increased sensorimotor network (SMN) gradient scores following nrTMS (Pre-TMS: -0.707 ± 0.108; Post-TMS: -0.636 ± 0.077; $p = 0.016$), and HH_SomMot_22 within upper limb motor cortex is most strongly correlated with motor recovery.

Conclusions: High-frequency nrTMS targeting the hand knob accelerated the motor recovery. Gradient analysis findings provide novel insights into therapeutic mechanisms of nrTMS and underscore the value of the hand knob as a stimulation target.

1. Introduction

Motor deficit often occurs after motor-related areas (primary motor cortex and supplementary motor area) glioma resection (Kim, 2013; Duffau and Capelle, 2004). Performing awake craniotomy (AC) can provide instant monitoring of motor function, but postoperative motor deficit could not be completely avoided (Rosenberg, 2010). A previous study reported that new or worsened postoperative motor deficits occurred in 60% of primary motor cortex (M1) glioma patients (Magill, 2018), even when awake craniotomy (AC) was performed, and that 38% of these motor deficits were permanent. More than 90% of SMA tumor resections were followed by motor deficit (Russell and Kelly, 2003). The

Abbreviations: AC, awake craniotomy; M1, Primary motor cortex; SMA, Supplementary motor area; fMRI, functional magnetic resonance imaging; nrTMS, neuro-navigated repetitive transcranial magnetic stimulation; FC, functional connectivity; FMA, Fugl-Meyer Assessment; EOR, extent of resection; rs-fMRI, resting-state functional magnetic resonance imaging; SMN, sensorimotor network; VIS, visual network; DAN, dorsal attention network; VAN, ventral attention network; LN, limbic network; FPC, frontoparietal control network; DMN, default mode network; PCC, posterior cingulate cortex; mPFC, medial prefrontal cortex; SFG, superior frontal gyrus; KS test, Kolmogorov–Smirnov test.

* Corresponding authors at: Peking Union Medical College Hospital (East), No.1 Shuaifuyuan, Wangfujing, Dongcheng District, Beijing, China (W. Ma). Beijing Tiantan Hospital, No. 119, South 4th Ring West Road, Fengtai District, Beijing, China (T. Jiang and S. Fang).

E-mail addresses: mawb@pumch.cn (W. Ma), taojiang1964@foxmail.com (T. Jiang), fangtuo1@aliyun.com (S. Fang).

https://doi.org/10.1016/j.nicl.2026.103981
Received 1 January 2026; Received in revised form 3 January 2026; Accepted 27 February 2026
Available online 4 March 2026
2213-1582/© 2026 The Author(s). Published by Elsevier Inc. This is an open access article under the CC BY-NC-ND license (http://creativecommons.org/licenses/by-nc-nd/4.0/).

prevention of motor deficits and the motor function recovery are critical for postoperative quality of life in glioma patients. AC, neuronavigation, task-based fMRI, and TMS tractography aim to prevent postoperative motor deficits, but specific rehabilitation methods for existing deficits remain limited (Sulangi, 2024; Muir, 2023).

Neuro-navigated repetitive TMS (nrTMS) modulates cortical excitability and promotes neuroplasticity following stroke (Jannati, 2023; Lefaucheur, 2020; Veldema, 2020). Unlike acute stroke, glioma patients experience preoperative functional compensation followed by secondary compensation after surgery (Duffau, 2020; Lv, 2022). Consequently, nrTMS rehabilitation strategies developed for stroke may not be directly applicable to glioma patients. Previous graph theoretical analyses revealed that the nodal efficiency of the hand knob area—in both fMRI-based functional and DTI-based structural brain networks—was correlated with motor recovery (Fang, 2025; Vassal, 2017; Fang, 2022). A small-sample study published by our research team on nrTMS targeting the ipsilateral hand knob demonstrated that high-frequency nrTMS could increase nodal efficiency of the stimulation site and accelerate motor recovery (Weng, 2024). However, the results require further validation, and the mechanisms of high-frequency nrTMS facilitating motor recovery remain unclear.

Functional gradient-based analysis has recently emerged as an influential method for investigating functional connectivity (FC) in resting-state fMRI. Unlike traditional voxel- or seed-based pairwise analysis, this approach reveals the spatial organization and continuous transitions across the cortex (Hong, 2020; Wang, 2025). Regions with similar connectivity profiles cluster along specific gradient axes, illustrating the fundamental dimension of an inherent coordinate system within the human cerebral cortex (Huntenburg et al., 2018). The principal gradient represents a hierarchical transition from primary sensorimotor functions to complex cognition functions, and reflects regional variations in connectivity patterns (Huntenburg et al., 2018). Functional gradients have become increasingly important for understanding the functional architecture of the brain and the pathophysiology of neurological disorders (Dong, 2023; Xiao, 2022; De Rosa, 2024). However, it remains unclear how functional gradients are altered in glioma patients with postoperative motor deficits. Also, the extent to which these alterations can be modulated by nrTMS is unknown. Therefore, principal gradients could offer insights into comprehensive network mechanisms and help elucidate how nrTMS accelerate motor function recovery.

This study applied high-frequency nrTMS targeting the hand knob to glioma patients with postoperative motor deficits and analyzed changes in principal gradients, potentially providing deeper insights into the therapeutic mechanisms of nrTMS.

2. Methods

2.1. Patient cohort

This single-centered randomized controlled trial study enrolled 30 patients who underwent resection of low-grade gliomas (based on WHO CNS 2016 criteria) involving motor-related areas were enrolled for nrTMS treatment at Beijing Tiantan Hospital between July 2023 and February 2025. This cohort was approved by the Ethics Committee on Scientific Research of the Hospital. The sample size was estimated based on our previous studies (Weng, 2024). Inclusion criteria were: (1) age $>$ 20 years; (2) no prior surgery or adjuvant therapy; (3) presence of contralateral upper or lower limb motor deficits following surgery; (4) right-handedness; (5) had AC glioma resection. Exclusion criteria included: (1) midline shift caused by the glioma; (2) excessive head motion ($>$1 mm translation or $>$ 1° rotation); (3) impaired consciousness or other serious postoperative complications preventing completion of MRI. All participants provided written informed consent before data collection. The randomization sequence was generated using a computer-based random number table. Patients assigned an odd number were allocated to the nrTMS group, while those assigned an even number were allocated to the sham group. Participants were blinded to their group assignment throughout the trial. The study was approved by the Ethics Committee on Scientific Research of Beijing Tiantan Hospital. Detailed descriptions of electromyography monitoring, motor mapping, and AC procedures during resection are provided in Supplementary Materials (Supplementary Methods Part 1). MRI data of healthy control participants (50 subjects) were obtained from the publicly available database, the Chinese Human Connectome Project (CHCP) (Ge, 2023).

2.2. Collection of demographic, clinical, and pathological data

Demographic, clinical, and pathological information was obtained from inpatient medical records. Tumor volume was measured using preoperative T2-FLAIR MRI sequences and calculated within the BrainLab neuro-navigation system. Extent of resection (EOR) was derived from pre- and postoperative MRI scans using the formula:

$$\mathrm{EOR} = \frac{\text{Preoperative volume} - \text{Postoperative volume}}{Peroperativevolume}$$

2.3. Experimental protocol

Patients exhibiting motor deficits by the seventh day after surgery were randomly allocated to nrTMS group or sham stimulation group (15 per group). Motor function was assessed using the Fugl-Meyer Assessment (FMA) and the UK Medical Research Council muscle strength grading at three time points: pre-intervention, post-intervention, and three months after intervention. Follow-up at 3 months was conducted via WeChat video if in-person evaluation was not feasible.

High-frequency nrTMS or sham nrTMS was delivered using a Magstim® device (England) guided by an ANT-neuro® navigation system (Netherlands). Stimulations were applied to the ipsilateral hand knob area of the precentral gyrus (Fig. 1A). The sham group received sham stimulation using a sham coil at the same location, mimicking the acoustic and tactile profile of an active coil at the set intensity and frequency without generating a transcranial magnetic stimulation. The resting motor threshold (rMT) was employed as the treatment stimulation intensity for each patient. rMT was defined as the minimal intensity over the hand knob required to elicit motor-evoked potentials $\geq$ 50 μV in the abductor pollicis brevis in $\geq$ 5 of 10 trials, using a figure-8 coil (Magstim®: 4150). The stimulation intensity was maintained at rMT throughout the treatment course, provided it was tolerable. No intolerance was reported in any subsequent sessions. Treatment was administered as three sessions everyday: session one targeted the hand knob of the motor cortex; session two targeted the site 1.5 cm superior to the hand area within the motor cortex; session three targeted the site 1.5 cm inferior to the hand area within the motor cortex, over seven consecutive days, starting on postoperative day seven or eight, within 24 h after postoperative imaging. Stimulation parameters followed previously established protocols (Lin, 2022; Naeser, 2005). Further procedural details are available in Supplementary Methods Part 2.

2.4. MRI data acquisition and preprocessing

Structural and functional MRI data were acquired on a 3.0 T MAGNETOM Prisma scanner (Siemens, Germany), including T1-3D, T2-FLAIR, and resting-state fMRI (rs-fMRI). Resting-state functional MRI (rs-fMRI) was performed using a single-shot echo-planar imaging (EPI) sequence with TR = 2000 ms, TE = 30 ms, FA = 75°, FOV = 220 × 220 mm^2, voxel size = 3.0 × 3.0 × 5.0 mm^3, and 30 slices. Sequence parameters are detailed in Supplementary Methods Part 3.

Preprocessing of rs-fMRI data was carried out with fMRIprep 23.2.3 (Esteban, 2019), with default parameters except for disabled slice timing correction and submillimeter reconstruction. Data was registered with a 2 mm MNI template. Subsequent processing involved spatial smoothing (6 mm FWHM) and high-pass temporal filtering (60 s cutoff) in FSL.

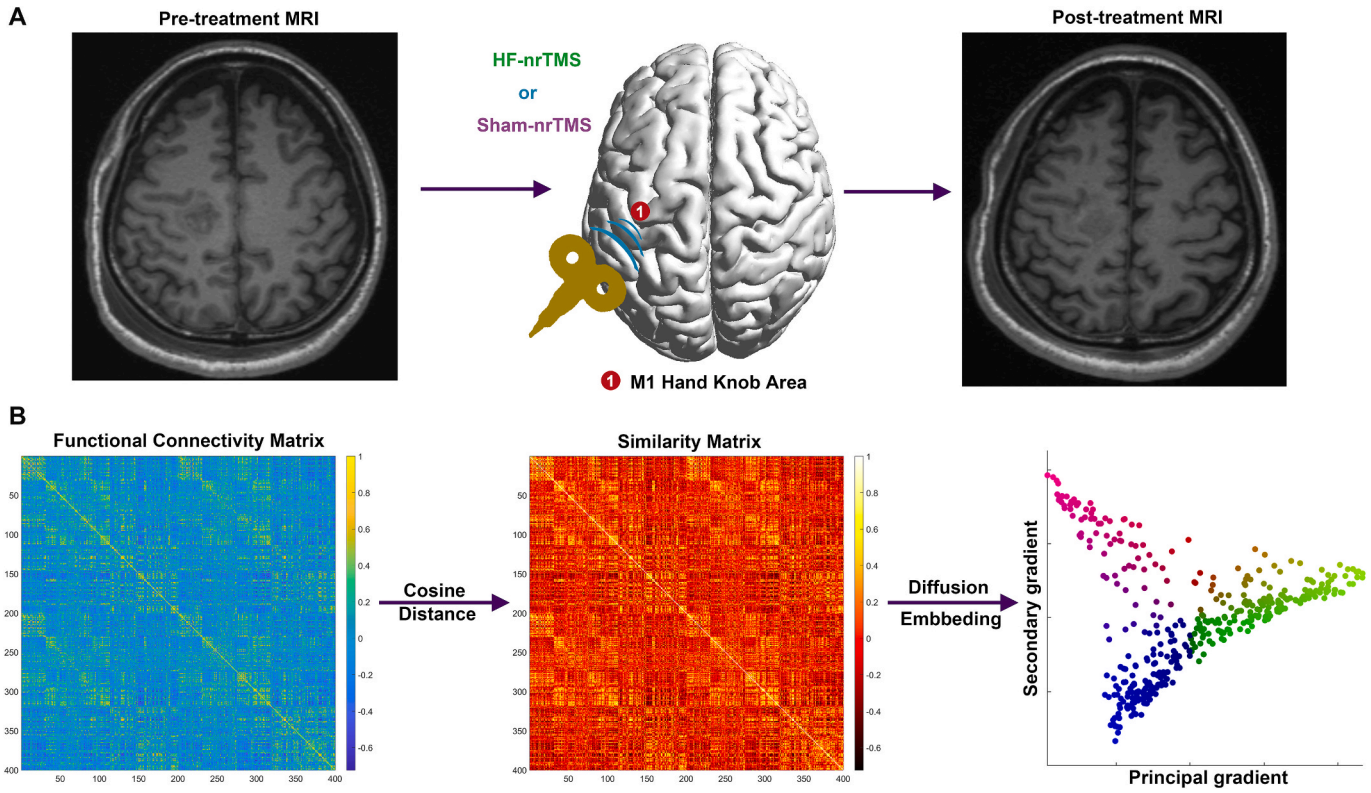

Fig. 1. A: Pipeline for nrTMS treatment; B: Pipeline for functional gradient processing: Functional connectivity matrices were derived through Pearson correlation. The connectivity matrix was subsequently converted into an affinity matrix, from which gradient components were extracted via diffusion embedding.

Registration outputs were adjusted according to recommended procedures for FSL–fMRIprep integration (Mumford, 2017). Following fMRIprep, the data were post-processed using XCP-D. Framewise displacement (FD) was calculated for each volume to control for motion artifacts (Power, 2014). Volumes with FD > 0.3 mm were flagged as high-motion outliers. then were subsequently censored and their time points were interpolated using the surrounding data after regression. Denoising was performed by regressing out 36 nuisance parameters, which included motion parameters, tissue signals, and their expansions and derivatives. The data were then band-pass filtered (0.01–0.08 Hz).

Although evidence for some hemispheric specialization and ipsilateral control exists, the dominant principle remains that limb control is strongly influenced by the contralateral primary motor system (Haaland and Harrington, 1996). Given our focus on comparing the tumor ipsilateral and contralateral sides, and most enrolled patients had tumors located in the left hemisphere (22/30), MRI images from patients with tumors located in the right hemisphere were flipped laterally to facilitate group-level analysis.

2.5. Gradient analysis

Time series were extracted from 400 nodes defined by the Schaefer400 atlas (Schaefer, 2018). Pairwise Pearson correlation matrices were converted to Z-scores via Fisher's transformation. Top 10% individual connectivity matrices were retained (Margulies, 2016). Diffusion map embedding transformed the high-dimensional relationships of connectivity profiles into distances to ensure a stable representation of connectivity patterns (Hong, 2020; Del Río, 2024). This process positioned network regions with similar patterns closer together spatially in the embedding space. Following recommendations from previous studies (Margulies, 2016), a manifold learning parameter of $\alpha = 0.5$ during diffusion embedding to preserve global relationships was applied. The first three components accounted for 37.4% (15.3%, 12.0%, 10.1% for nrTMS group; 15.4%, 11.9%, 10.1% for sham group) of the variance.

For each resulting gradient map, three global metrics were computed: variance, range, and explanation ratio. The explanation ratio quantifies the percentage of connectivity variance explained by a specific gradient; a higher ratio indicates that the corresponding embedding axis captures a more dominant organizational pattern within the functional connectome. The principal gradient—capturing the largest variance in connectivity—was extracted for subsequent analysis (Hong, 2019; Guo, 2023) (Fig. 1B).

Network gradient values were averaged within major functional networks—visual (VIS), sensorimotor (SMN), dorsal attention (DAN), ventral attention (VAN), limbic (LN), frontoparietal (FPC), and default mode network (DMN) (Yeo, 2011). The average parcel gradient within a network was determined as the network gradient. Within-network dispersion was the median score of the Euclidean distance from each parcel gradient score to the network centroid. Between-network dispersion was the Euclidean distance between the centroids of networks (Shen, 2023).

2.6. Statistical analysis

Demographic variables were compared using independent for continuous data and chi-square tests for categorical measures. Shapiro-Wilk test was used for normality for individual gradient distribution and parcel gradient score distribution. Statistical analysis of variables (FMA score, muscle strength) measured at multiple time points was performed using repeated-measures ANOVA. Group differences in clinical scores were assessed via independent t-tests; within-group changes were evaluated with paired t-tests. Gradient changes were examined at global, network, and parcel levels. The Kolmogorov–Smirnov (K–S) test compared global gradient distributions (Whitley and Ball, 2002). For the global gradient metrics, the statistical significance threshold was set at $P < 0.05$. Parcel-level differences within network used t-tests with significance thresholds set at P values of < 0.05 after FDR correction

(Bassett, 2009). The number of statistical tests for each network was determined by its constituent parcels: 61 for VIS; 77 for SMN; 46 for DAN; 47 for VAN; 26 for LN; 52 for the FPC; and 91 for DMN. Motor function-related gradients were further selected using LASSO regression (Li and Sillanpää, 2012). Correlations were evaluated using Pearson or Spearman coefficients.

3. Results

3.1. Demographic characteristics and clinical outcomes

A total of 30 patients who underwent resection of low-grade gliomas (based on WHO CNS 2016 criteria) involving motor-related areas were enrolled, nrTMS group and sham stimulation group had fifteen patient each. Demographic, clinical, and pathological characteristics patients are present in Supplementary Table 1, and no significant difference was found in age, tumor volume, EOR, Gender, MGMT promoter methylation, IDH status, 1p/19q status, and adjuvant therapy condition between nrTMS group and sham stimulation group. The tumor overlapping results are shown in Supplementary Fig. 1.

Repeated-measures ANOVA revealed significant differences between the nrTMS and Sham groups over time. For muscle strength, a significant main effect of treatment was observed ($F = 4.216$, $p = 0.049$, $\eta p^2 = 0.040$). Significant and predominant effect of time was also found in both muscle strength and FMA score measures. Significant Group × Time interaction indicated that the pattern of improvement over time differed between the two groups in muscle strength and FMA score (muscle strength: $F = 7.574$, $p = 0.001$; FMA score: $F = 3.553$, $p = 0.035$; Table 1). Results of post hoc tests (sidak's multiple comparisons) revealed muscle strength for each time point are significantly better in nrTMS group (Post-treatment: nrTMS: 3.533 ± 0.720, Sham: 2.067 ± 0.572, $p = 0.019$, $d = 1.082$; 3-month follow-up: nrTMS: 4.600 ± 0.408, Sham: 3.733 ± 0.609, $p = 0.035$, $d = 1.012$) (Fig. 2).

3.2. Gradients differences between patients and healthy controls

Global-level gradient scores were calculated for both patients and healthy controls to characterize cortical organization, and significant parcels are represented on the cortical surface (Fig. 3A). Shapiro-Wilk test indicated a non-normal distribution of the principal gradient in all tumor patients (Supplementary Table 2). The parcel gradient score distribution across samples was generally consistent with normality (89% for pre-TMS; 89.5% for post-TMS; 86.5% for pre-Sham; 88.2% for post-Sham are normally distributed, Supplementary Fig. 2A-B). No baseline differences were found at the network level between the nrTMS and sham groups, and at the parcel level (Supplementary Table 3), only four regions survived FDR correction (HH_Default_pCunPCC_7, LH_Default_pCunPCC_9, HH_Default_pCunPCC_6, HH_DorsAttn_Post_16), which are located in the posterior cingulate cortex and superior parietal lobule (Supplementary Fig. 2C). The distribution of the principal gradient demonstrated significant and diverse differences between patients and healthy controls (KS Test: $D = 0.120$, $p = 0.006$) (Supplementary Fig. 3). Suggesting disrupted cortical organization associated with the effects of tumor and the surgical procedure.

At the network level, significant differences in principal gradient scores were observed between patient and control groups: the SMN (healthy control: −0.777 ± 0.047; patient: −0.596 ± 0.041, $p < 0.0001$, $d = 1.192$) and the VAN (healthy control: −0.349 ± 0.048; patient: −0.263 ± 0.051, $p = 0.015$, $d = 0.507$) showed significantly increased scores in patients, while the VIS (healthy control: −0.903 ± 0.048; patient: −1.009 ± 0.053, $p = 0.004$, $d = -0.604$), LN (healthy control: 0.651 ± 0.058; patient: −0.596 ± 0.041, $p < 0.0001$, $d = -1.141$), and DMN (healthy control: 1.145 ± 0.027; patient: 1.033 ± 0.039, $p < 0.0001$, $d = -0.976$) exhibited significantly decreased scores compared to healthy controls (Fig. 3A-B).

3.3. Macroscale gradient alteration after nrTMS treatment

Global-level gradient scores were calculated for the nrTMS group and the sham stimulation group to characterize cortical organization, visually represented on the cortical surface (Fig. 4A). After nrTMS treatment, narrowing of the distribution was observed compared with the Pre-TMS and sham group distributions (Pre-Sham/Post- Sham: KS Test: $d = 0.068$, $p = 0.312$; Post-TMS/Pre-TMS KS Test: $d = 0.045$, $p = 0.804$) (Fig. 4B). At the network level, the gradient scores of the SMN demonstrated a significant increase following nrTMS treatment (Pre-TMS: −0.707 ± 0.108; Post-TMS: −0.636 ± 0.077; $p = 0.016$, $d = 0.758$). In contrast, no significant changes were observed in any networks after sham stimulation, including the SMN (Fig. 4C-D). Within-network dispersion decreased in the SMN, VIS, LN, FPC, and DMN, but only the LN showed a significant reduction in both nrTMS group (Pre-TMS: 0.027 ± 0.004; Post-TMS: 0.022 ± 0.002p = 0.018, d = -0.773) and sham group (Pre-Sham: 0.027 ± 0.004; Post-Sham: 0.021 ± 0.002, $p = 0.015$, $d = -0.766$). For between-network dispersion, only the DMN exhibited a significant reduction (Fig. 4E-F) (Pre-TMS: 0.058 ± 0.008; Post-TMS: 0.050 ± 0.007, $p = 0.005$, $d = -0.945$), and there is no significant result in sham group.

3.4. Gradient alteration at the parcel-level after nrTMS treatment

Parcel-level gradient scores for the Post-TMS and Pre-TMS sessions were calculated for the nrTMS group, and the significant parcels are listed in Table 2. The sham group exhibited fewer significant parcels (Supplementary Table 4). These parcels primarily originated from two networks: SMN and DMN. Within the SMN, four significant parcels were identified in nrTMS group, whereas none were found in the sham group. Among these, three parcels located in M1 showed significantly increased gradient scores (upper limb motor areas: LH_SomMot_19 and HH_SomMot_22; facial motor area: HH_SomMot_12), while one parcel located in the postcentral gyrus (LH_SomMot_32) exhibited a significantly decreased gradient score (Fig. 5A-B). Within the DMN, all significant parcels demonstrated significantly increased gradient scores in nrTMS group (Fig. 5C-D). These parcels were distributed across several regions, including the posterior cingulate cortex (PCC), precuneus, medial prefrontal cortex (mPFC), and superior frontal gyrus (SFG).

Table 1
ROIs with significant changes after nr-TMS treatment.

Measure	Pre-treatment	Post-treatment	3-month follow-up	Group	Time	Group × Time
Muscle strength						
nrTMS	1.067 ± 0.552	3.533 ± 0.720	4.600 ± 0.408	F (1, 28) = 4.216	F (1.98, 55.5) = 159.9	F (2, 56) = 7.574
Sham	0.933 ± 0.677	2.067 ± 0.572	3.733 ± 0.609	P=0.049* ηp^2=0.040	P<0.0001 ηp^2=0.567	P=0.001*
FMA score						
nrTMS	18.600 ± 16.003	70.200 ± 8.380	91.867 ± 3.707	F (1, 28) = 2.351	F (1.83, 51.2) = 118.2	F (2, 56) = 3.553
Sham	17.000 ± 14.252	45.800 ± 9.562	81.867 ± 8.347	P=0.137 ηp^2=0.023	P<0.0001 ηp^2=0.556	P=0.035*

Abbreviations: ηp^2, partial eta-squared. Data are presented as mean with 95% confidence interval, the reported F and p values for Time are Greenhouse-Geisser corrected.

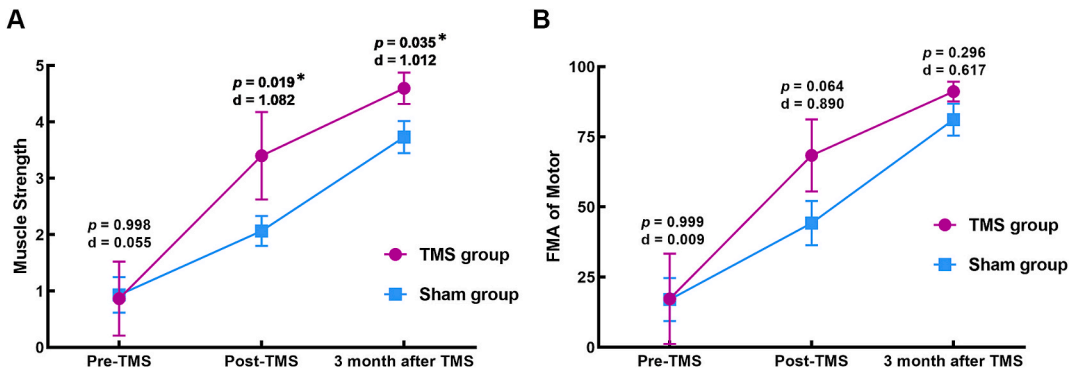

Fig. 2. A: Changes in FMA scores in the nrTMS and sham groups; B: Changes in muscle strength in the nrTMS and sham groups. FMA: Fugl-Meyer Assessment. Sidak's multiple comparisons *p < 0.05.

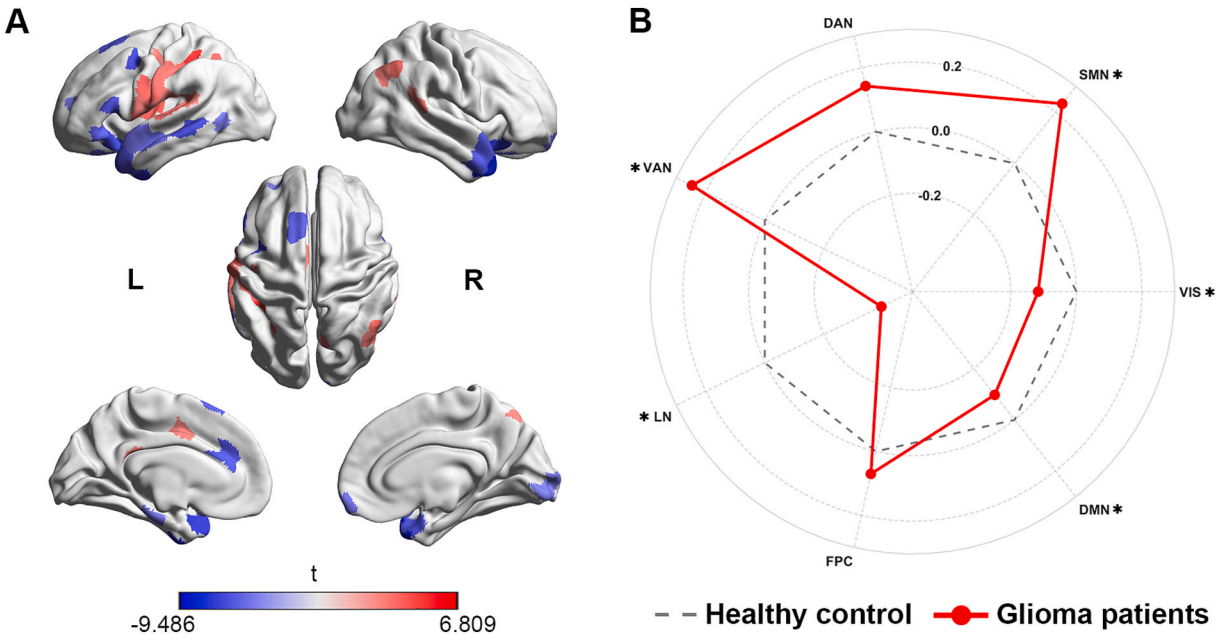

Fig. 3. Comparisons between glioma patients and healthy control. A: Cortical surface maps showing regions with significant inter-group differences; B: The radar chart illustrates the gradient Z-scores of subnetworks for each group, normalized to control values. VIS, visual network; SMN, somatomotor network; DAN, dorsal attention network; VAN, ventral attention network; LN, limbic network; FPC, frontoparietal network; DMN, default mode network; *p < 0.05.

3.5. Selection of motor function recovery-associated parcels and correlation analysis

LASSO regression (20/30 samples, 10 were randomly selected from each group) was employed to identify most strongly associated with muscle strength variations among all significant parcels of Post-TMS and Pre-TMS sessions.

The optimal regularization parameter was determined via 10-fold cross-validation, selecting variables with non-zero coefficients. The results indicated LH_SomMot_19 and HH_SomMot_22, both located in upper limb motor areas, exhibited the strongest positive association with motor function recovery, and LH_Default_pCunPCC_7 exhibited negative correlation (Fig. 6A-C). The resulting linear model takes the form:

$$\Delta\text{muscle strength} = 2.2284 + 11.0168 \times \Delta\text{HH\_SomMot\_22} + 3.912 \times \Delta\text{LH\_SomMot\_19} - 2.1478 \times \Delta\text{LH\_Default\_pCunPCC\_7}.$$

Model performance was evaluated on the validation set (10/30 samples) using R^2 and RMSE (Fig. 6D). The LASSO model identified key predictors of motor recovery, but the limited sample size likely contributed to modest performance and unstable estimates, larger validation studies are needed. Spearman correlation analysis demonstrated a significant correlation between gradient score variations and improvement in muscle strength in HH_SomMot_22 (HH_SomMot_22: r = 0.427, p = 0.019; Fig. 6E). Patients in the TMS group were further divided into fast (upper 50%) and slow-recovery (lower 50%) groups according to their FMA score increase, we compared the primary gradient variation of HH_SomMot_22 and found no significant difference (fast-recovery: 0.024 ± 0.019; slow-recovery: 0.007 ± 0.018, p = 0.140).

4. Discussion

This study investigated functional gradient patterns in glioma patients with postoperative motor deficits, with tumors involving M1, SMA, or CST. Following high-frequency nrTMS targeting the hand knob, a pivotal outcome was an acceleration of motor function recovery, consistent with our previous study (Weng, 2024). This facilitatory effect on motor function recovery was particularly significant in the early postoperative period, as reflected in both FMA scores and muscle strength, and patients in the nrTMS group maintained significantly better muscle strength compared to the sham group three months after treatment. These findings underscore the therapeutic potential of high-frequency nrTMS targeting the hand knob for postoperative motor

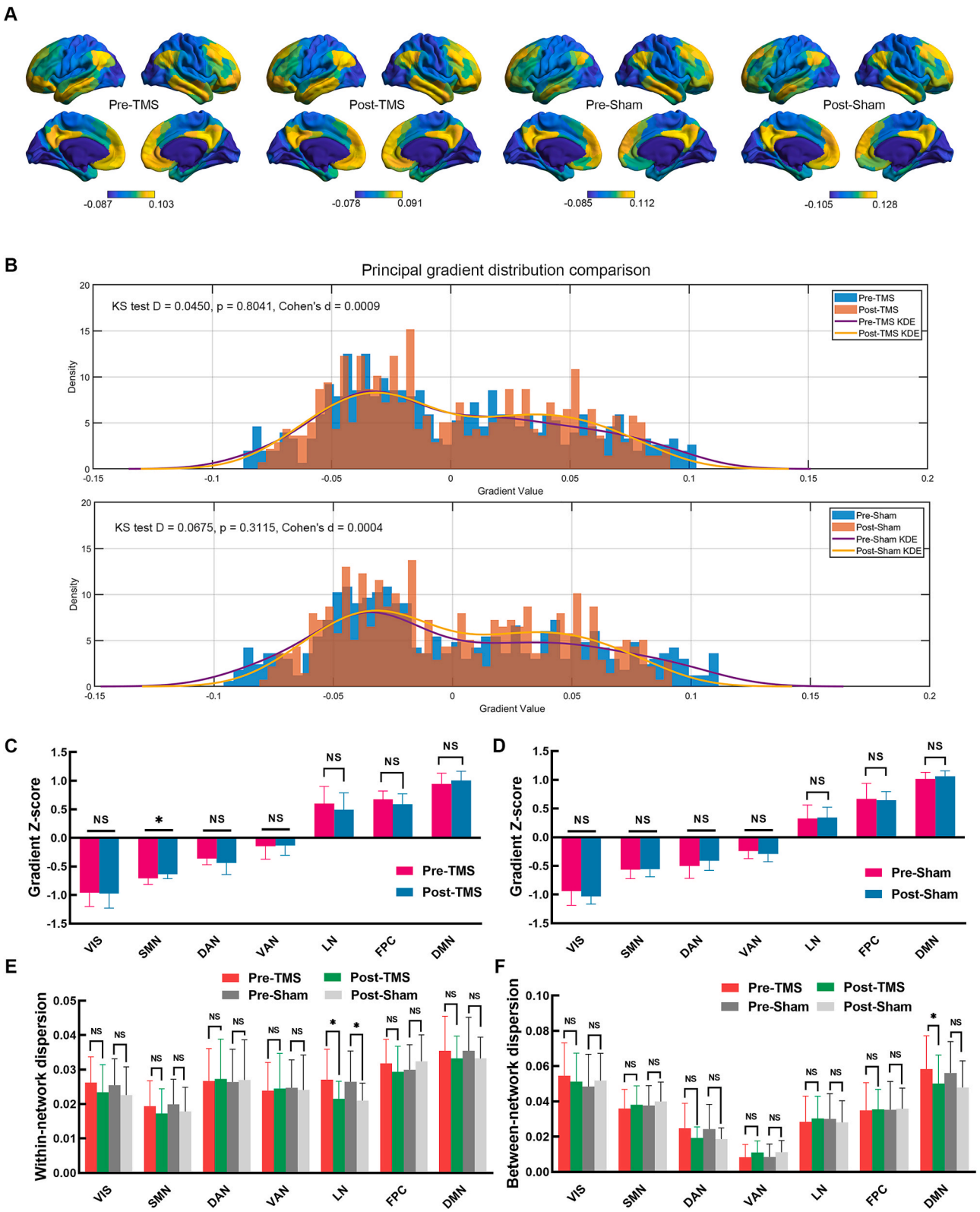

Fig. 4. Global and network-level comparisons of the principal gradient scores across groups. A. The group-average principal functional gradient of Pre-TMS, Post-TMS, and sham groups; B: Global histogram of nrTMS and sham group; C: Bar graph representation of the principal gradient scores for subnetworks between Pre-TMS and Post-TMS groups; D: Bar graph representation of the principal gradient scores for subnetworks between Pre-Sham and Post-Sham groups; E: Within-network comparison of principal gradient scores between Pre-TMS and Post-TMS groups; F: Between-network dispersion comparison of principal gradient scores between Pre-TMS and Post-TMS groups. L, lesion; H, healthy; VIS, visual network; SMN, somatomotor network; DAN, dorsal attention network; VAN, ventral attention network; LN, limbic network; FPC, frontoparietal network; DMN, default mode network; *p < 0.05; NS, Not Significant.

Table 2
ROIs with significant changes after nr-TMS treatment.

ROI name	Position	Cohen's d	Pre-TMS	Post-TMS	FDR p adj
LH_SomMot_19	M1	0.833	-0.057 ± 0.006	-0.036 ± 0.013	0.040
LH_SomMot_32	S1	-0.684	-0.026 ± 0.013	-0.048 ± 0.013	0.035
RH_SomMot_22	M1	0.954	-0.053 ± 0.007	-0.036 ± 0.008	0.040
RH_SomMot_12	M1	1.245	-0.037 ± 0.005	-0.023 ± 0.005	0.040
LH_Default_pCunPCC_7	PCC	0.977	0.069 ± 1.620	0.101 ± 0.970	0.028
LH_Default_pCunPCC_11	PCUN	0.550	0.049 ± 1.907	0.074 ± 1.926	0.045
LH_Default_PFC_3	mPFC	0.760	0.075 ± 0.646	0.092 ± 1.081	0.032
RH_Default_pCunPCC_6	PCC	0.949	0.078 ± 0.929	0.098 ± 0.815	0.032
RH_Default_pCunPCC_2	PCC	0.720	0.048 ± 1.836	0.075 ± 1.309	0.032
RH_Default_PFCdPFCm_4	mPFC	0.699	0.082 ± 0.890	0.098 ± 1.104	0.032
RH_Default_PFCdPFCm_11	SFG	0.767	0.073 ± 0.688	0.090 ± 1.147	0.032
RH_Limbic_TempPole_3	Temporal pole	-0.690	0.029 ± 1.341	0.005 ± 1.452	0.041
LH_DorsAttn_Post_13	SPL	-0.925	-0.020 ± 1.540	-0.052 ± 1.347	0.015

Abbreviations: M1, precentral gyrus; S1, postcentral gyrus; PCC, posterior cingulate cortex; PCUN, precuneus; mPFC, medial prefrontal cortex; SFG, superior frontal gyrus; SPL, Superior Parietal Lobule. Data are presented as mean with 95% confidence interval.

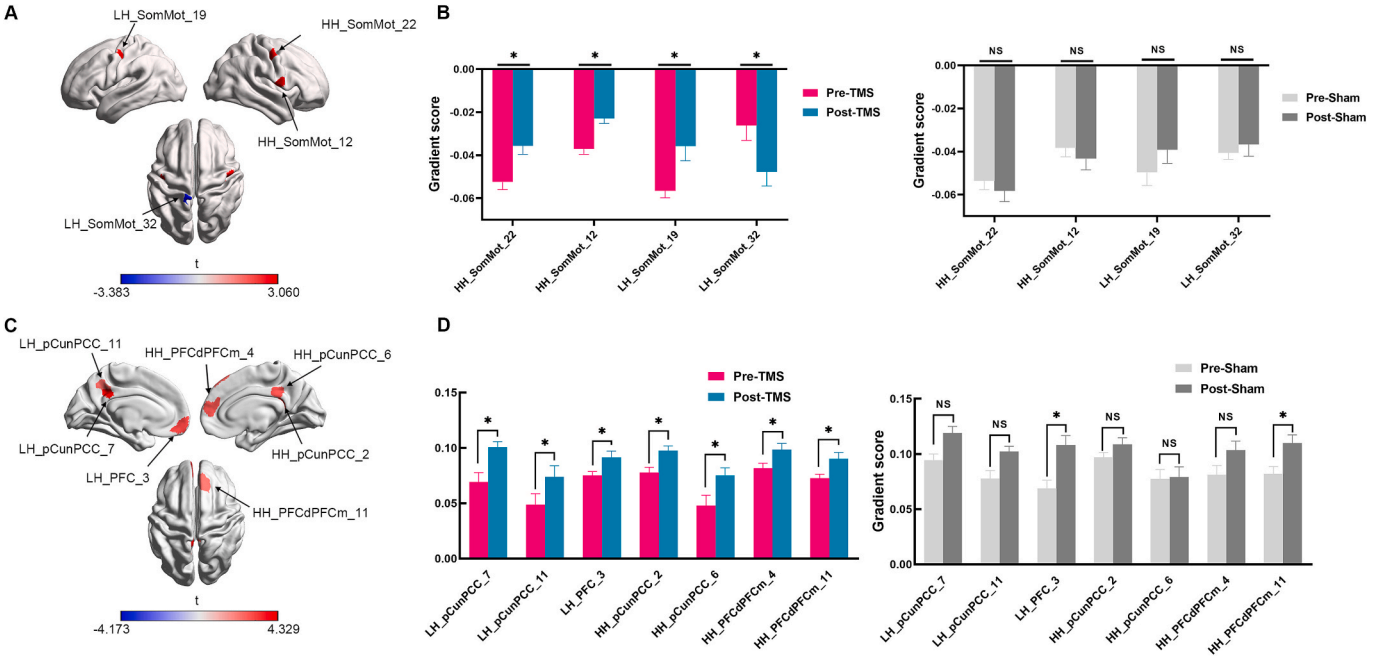

Fig. 5. Parcel-level comparisons of the principal gradient scores between Pre-TMS and Post-TMS groups. A: Cortical surface maps showing regions with significant inter-group differences within SMN; B: Bar graph representation of regions with significant inter-group differences within SMN; C: Cortical surface maps showing regions with significant inter-group differences within DMN; D: Bar graph representation of regions with significant inter-group differences within DMN. SMN, somatomotor network; DMN, default mode network; *p < 0.05 FDR correction.

deficits after glioma resection.

The global distribution of the principal gradient in patients and healthy controls exhibited significant distinct topological patterns, and most significant parcels were located in the SMN, DMN, and LN. This distribution variation may be attributed to tumor infiltration and surgical intervention, but the inconsistency in rs-fMRI acquisition protocols and scan length between the patient and healthy control groups could also contribute to the observed differences, so more rigorously controlled studies are needed. At the network level, significant differences in principal gradient scores were observed in the SMN, VAN, VIS, LN, and DMN. Specifically, patients demonstrated significantly increased principal gradient scores in the SMN compared to healthy controls. The increased principal gradient scores suggest shifts of the SMN toward more multimodal and active states (Jiang, 2024). The SMN have undergone gradual compensation during tumor growth, which commenced even before motor deficits occurred (Duffau, 2005). These observations are consistent with the notion that the increase in principal gradient scores of the SMN may manifest the compensation of the SMN during tumor infiltration. Additionally, the principal gradient distribution in patients still adhered to the established conceptual framework wherein gradients form a continuum from unimodal sensory cortices to transmodal association regions, indicating that this hierarchical gradient organization is fundamental and relatively conserved (Felleman and Van Essen, 1991; Setton, 2022; Guo, 2025; Zhang, 2022).

Following high-frequency nrTMS treatment, there was a non-significant trend toward narrowing the global principal gradient distribution. The result aligns with earlier research examining functional gradients after TMS treatment (Xie, 2024). Previous studies have indicated that low-frequency rTMS can regulate cortical connectivity and alleviate symptoms in multiple psychiatric conditions (Xie, 2024; Tan, 2023; Xie, 2024; Blumberger, 2018). The narrowing of the principal gradient distribution following nrTMS treatment, reflecting a trend toward cortical normalization, implies that nrTMS could induce sustained adjustments in cortical excitability through possible mechanisms like long-term depression and long-term potentiation (Lenz, 2016; Galanis, 2025).

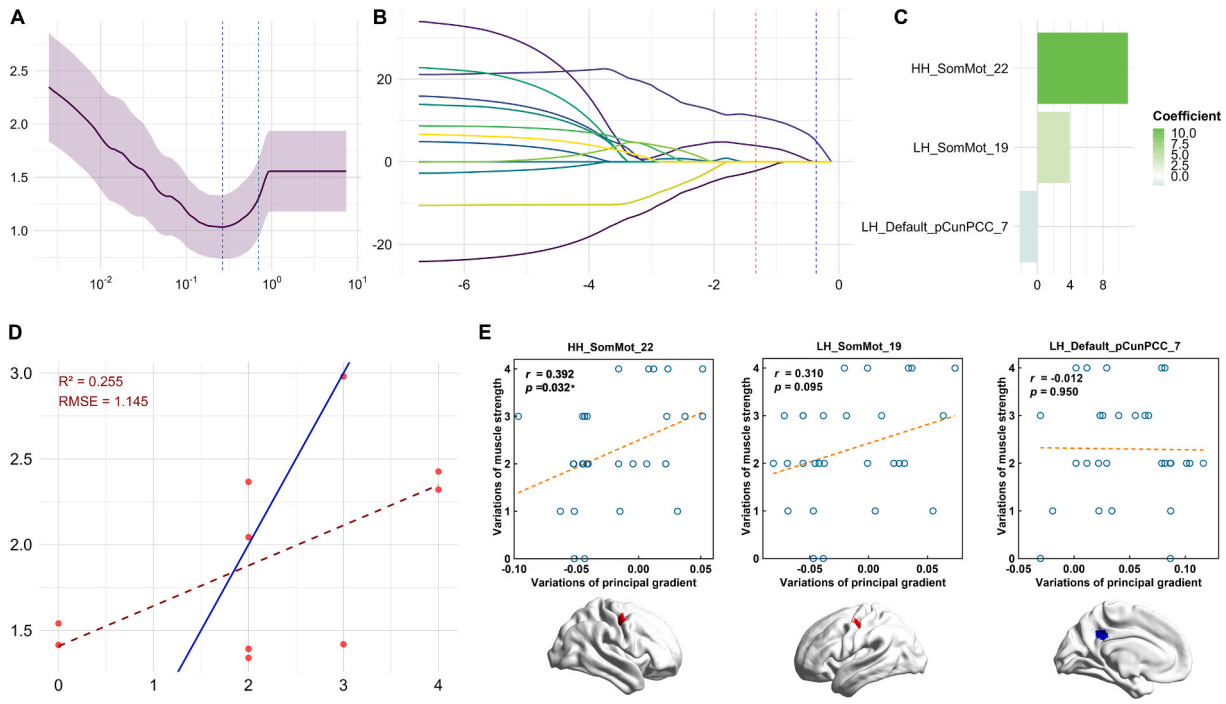

Fig. 6. Selection of motor function recovery-associated parcels and correlation analysis. A: Least absolute shrinkage and selector operation (LASSO) coefficient profiles of all significant parcels; B: Ten-fold cross-validation for tuning parameter selection in the LASSO model for analysis of the correlation between the regional principal gradient variation and muscle strength variation; C: Coefficient of selected regional principal gradient; D: Performance of the LASSO-derived muscle strength recovery prediction model in the validation set; E: Correlation between HH_SomMot_22 principal gradient variation and muscle strength variation.

At the network level, the SMN was the only network that exhibited a significant increase in gradient scores following nrTMS, whereas no significant changes were observed in any networks of the sham group. The alterations of the SMN after nrTMS treatment were consistent with the tumor patients/healthy controls analysis, potentially reflecting motor function compensatory processes. The SMN plays a critical role in sensorimotor integration (Rao, 2024) and includes postcentral gyrus, precentral gyrus, and supplementary motor areas (Gorges, 2017), The results suggest principal gradient score of SMN may reflect the compensatory states of motor function.

Further parcel-level analysis revealed that brain regions with significant changes after nrTMS were predominantly located in the SMN and the DMN. HH_SomMot_22 was the most positively correlated with motor function recovery (the healthy hemisphere upper limb motor area within the hand knob). The principal gradient score of a parcel represents its connectivity pattern (Samara, 2023). Previous studies have shown that rTMS targeting the temporoparietal junction is associated with metabolic and connectivity changes in the contralateral cortex (Bais, 2017), suggesting TMS may indirectly influence the contralateral hemisphere (Xie, 2023). Similar effect was observed in this study: stimulation targeting the ipsilateral hand knob resulted in increased gradient values not only in the ipsilateral but also in the contralateral upper limb motor areas. These results underscore the ability of nrTMS to modulate bilateral brain networks and highlight the pivotal role of upper limb motor areas in motor recovery, consistent with previous findings from functional graph theoretical analyses and structural network studies. Additionally, following TMS treatment, significant increases in gradient values were also detected in DMN regions such as the PCC and mPFC. The PCC and mPFC are integral to emotional and cognitive processes (Vogt;, 2005; Guo, 2024). One study reported that rTMS targeting the mPFC improved sleep quality in patients with insomnia (Sun, 2022).

Network dispersion analysis revealed that the within-network dispersion of principal gradient scores decreased after nrTMS across networks except DAN and VAN, these changes were not significant except in the LN. Lower dispersion suggest more homogeneous connectivity patterns within these networks. A significant reduction in between-network dispersion was observed in DMN, indicating stronger integration between the DMN and other networks.

5. Limitations

This study has several limitations. First, it is a single-center exploratory study with a relatively small sample size, which may limit the generalizability of the findings. Second, the spatial resolution of the resting-state fMRI data (5-mm slice thickness) is relatively coarse for gradient mapping, a technique sensitive to anatomical detail, which may affect the precision of the results. Third, despite enrolling only patients with low-grade gliomas in motor-related cortex, heterogeneity in tumor size and location inherently contributed to variance in gradient distribution, a fundamental challenge in neuro-oncological research. Future multi-center studies with larger samples, optimized imaging protocols, and advanced methods to account for tumor heterogeneity are warranted to validate and refine these findings.

6. Conclusion

High-frequency nrTMS targeting the hand knob accelerated the motor recovery. Gradient analysis revealed increased SMN gradient scores following nrTMS, and HH_SomMot_22 (the healthy hemisphere upper limb motor area within the hand knob) is most strongly correlated with motor recovery. This study provides valuable perspective on the functional gradient of cortical organization in the context of high-frequency nrTMS treatment, potentially shedding light on the therapeutic mechanisms of high-frequency nrTMS, and validates the therapeutic value of the hand knob as a stimulation target.

8. Consent for publication

Written informed consent was obtained from all participants.

CRediT authorship contribution statement

Yuzhe Li: Writing – review & editing, Writing – original draft, Visualization, Validation, Software, Methodology, Investigation, Formal analysis. **Jiangwei Wang:** Software, Investigation. **Zhong Zhang:** Investigation. **Xing Fan:** Investigation. **Yinyan Wang:** Investigation. **Wenbin Ma:** Supervision. **Tao Jiang:** Writing – review & editing, Supervision, Funding acquisition. **Shengyu Fang:** Writing – review & editing, Methodology, Investigation, Formal analysis, Data curation.

7. Ethics approval and consent to participate

This research was approved by the Ethics Committee on Scientific Research of Beijing Tiantan Hospital, Capital Medical University (approval number: KY-2022-206-03).

Funding

This study was supported by funds as follows: Beijing Research Ward Excellence Program (BRWEP2024W032040210); National Natural Science Foundation of China (No. 82203170); Beijing Natural Science Foundation (No. JQ23040); Non-profit Central Research Institute Fund of Chinese Academy of Medical Sciences, the National High Level Hospital Clinical Research Funding (2025-PUMCH-A-158); Brain Tumor Precision Diagnosis and Treatment and Translational Medicine Innovation Unit, Chinese Academy of Medical Sciences (2019-I2M-5-021).

Declaration of competing interest

The authors declare that they have no known competing financial interests or personal relationships that could have appeared to influence the work reported in this paper.

Acknowledgements

Not applicable.

Trial registry

Accelerating Motor Recovering in Patients With SMA Syndrome After Glioma Surgery by Using nrTMS: NCT05803057

Appendix A. Supplementary data

Supplementary data to this article can be found online at https://doi.org/10.1016/j.nicl.2026.103981.

Data availability

Data will be made available on request.

References

Kim, Y.H., et al., 2013. Risk factor analysis of the development of new neurological deficits following supplementary motor area resection. J. Neurosurg. 119 (1), 7–14.
Duffau, H., Capelle, L., 2004. Preferential brain locations of low-grade gliomas. Cancer 100 (12), 2622–2626.
Rosenberg, K., et al., 2010. Prediction of neurological deficits and recovery after surgery in the supplementary motor area: a prospective study in 26 patients. J. Neurosurg. 113 (6), 1152–1163.
Magill, S.T., et al., 2018. Resection of primary motor cortex tumors: feasibility and surgical outcomes. J. Neurosurg. 129 (4), 961–972.
Russell, S.M. and P.J. Kelly, Incidence and clinical evolution of postoperative deficits after volumetric stereotactic resection of glial neoplasms involving the supplementary motor area. Neurosurgery, 2003. **52**(3): p. 506-16; discussiom 515-6.
Sulangi, A.J., et al., 2024. Neuronavigation in glioma resection: current applications, challenges, and clinical outcomes. Front. Surg. 11, 1430567.
Muir, M., et al., 2023. Comparative study of preoperative functional imaging combined with tractography for prediction of iatrogenic motor deficits. J. Neurosurg. 139 (1), 65–72.
Jannati, A., et al., 2023. Assessing the mechanisms of brain plasticity by transcranial magnetic stimulation. Neuropsychopharmacology 48 (1), 191–208.
Lefaucheur, J.P., et al., 2020. Evidence-based guidelines on the therapeutic use of repetitive transcranial magnetic stimulation (rTMS): an update (2014-2018). Clin. Neurophysiol. 131 (2), 474–528.
Veldema, J., et al., 2020. Noninvasive brain stimulation in rehabilitation of hemispatial neglect after stroke. CNS Spectr. 25 (1), 38–49.
Duffau, H., 2020. Functional Mapping before and after Low-Grade Glioma Surgery: a New Way to Decipher Various Spatiotemporal patterns of Individual Neuroplastic potential in Brain Tumor patients. Cancers (Basel) 12 (9).
Lv, K., et al., 2022. Neuroplasticity of Glioma patients: Brain Structure and Topological Network. Front. Neurol. 13, 871613.
Fang, S., et al., 2025. The Variation of White Matter Connectome after Surgery Revealed Factors Affecting Supplementary Syndrome Recovery Time in Low-Grade Glioma patients. CNS Neurosci. Ther. 31 (5), e70426.
Vassal, M., et al., 2017. Recovery of functional connectivity of the sensorimotor network after surgery for diffuse low-grade gliomas involving the supplementary motor area. J. Neurosurg. 126 (4), 1181–1190.
Fang, S., et al., 2022. Increasing nodal vulnerability and nodal efficiency implied recovery time prolonging in patients with supplementary motor area syndrome. Hum. Brain Mapp. 43 (13), 3958–3969.
Weng, S., et al., 2024. Postoperative Nodal Efficiency of the Lesional-Hemispheric Hand Motor Area increasing Potentially Facilitated Motor Recovery for SMA Syndrome. CNS Neurosci. Ther. 30 (11), e70112.
Hong, S.J., et al., 2020. Toward a connectivity gradient-based framework for reproducible biomarker discovery. Neuroimage 223, 117322.
Wang, Y., et al., 2025. Multimodal gradients unify local and global cortical organization. Nat. Commun. 16 (1), 3911.
Huntenburg, J.M., Bazin, P.L., Margulies, D.S., 2018. Large-Scale Gradients in Human Cortical Organization. Trends Cogn. Sci. 22 (1), 21–31.
Dong, D., et al., 2023. Compressed sensorimotor-to-transmodal hierarchical organization in schizophrenia. Psychol. Med. 53 (3), 771–784.
Xiao, Y., et al., 2022. Charting the dorsal-medial functional gradient of the default mode network in major depressive disorder. J. Psychiatr. Res. 153, 1–10.
De Rosa, A.P., et al., 2024. Functional gradients reveal cortical hierarchy changes in multiple sclerosis. Hum. Brain Mapp. 45 (6), e26678.
Ge, J., et al., 2023. Increasing diversity in connectomics with the Chinese Human Connectome Project. Nat. Neurosci. 26 (1), 163–172.
Lin, B.F., et al., 2022. Functional Remodeling Associated with Language Recovery after Repetitive Transcranial magnetic Stimulation in Chronic Aphasic Stroke. Front. Neurol. 13, 809843.
Naeser, M.A., et al., 2005. Improved picture naming in chronic aphasia after TMS to part of right Broca's area: an open-protocol study. Brain Lang. 93 (1), 95–105.
Esteban, O., et al., 2019. fMRIPrep: a robust preprocessing pipeline for functional MRI. Nat. Methods 16 (1), 111–116.
Mumford, J.A., 2017. A comprehensive review of group level model performance in the presence of heteroscedasticity: can a single model control Type I errors in the presence of outliers? Neuroimage 147, 658–668.
Power, J.D., et al., 2014. Methods to detect, characterize, and remove motion artifact in resting state fMRI. Neuroimage 84, 320–341.
Haaland, K.Y., Harrington, D.L., 1996. Hemispheric asymmetry of movement. Curr. Opin. Neurobiol. 6 (6), 796–800.
Schaefer, A., et al., 2018. Local-Global Parcellation of the Human Cerebral Cortex from Intrinsic Functional Connectivity MRI. Cereb. Cortex 28 (9), 3095–3114.
Margulies, D.S., et al., 2016. Situating the default-mode network along a principal gradient of macroscale cortical organization. PNAS 113 (44), 12574–12579.
Del Río, M., et al., 2024. Higher Sensory Sensitivity is Linked to Greater expansion Amongst Functional Connectivity Gradients. J. Autism Dev. Disord. 54 (1), 56–74.
Hong, S.J., et al., 2019. Atypical functional connectome hierarchy in autism. Nat. Commun. 10 (1), 1022.
Guo, S., et al., 2023. Functional gradients in prefrontal regions and somatomotor networks reflect the effect of music training experience on cognitive aging. Cereb. Cortex 33 (12), 7506–7517.
Yeo, B.T., et al., 2011. The organization of the human cerebral cortex estimated by intrinsic functional connectivity. J. Neurophysiol. 106 (3), 1125–1165.
Shen, Y., et al., 2023. Functional connectivity gradients of the cingulate cortex. Commun. Biol. 6 (1), 650.
Whitley, E., Ball, J., 2002. Statistics review 6: Nonparametric methods. Crit. Care 6 (6), 509–513.
Bassett, D.S., et al., 2009. Cognitive fitness of cost-efficient brain functional networks. PNAS 106 (28), 11747–11752.
Li, Z., Sillanpää, M.J., 2012. Overview of LASSO-related penalized regression methods for quantitative trait mapping and genomic selection. Theor. Appl. Genet. 125 (3), 419–435.
Jiang, Y., et al., 2024. Identifying individual brain development using multimodality brain network. Commun. Biol. 7 (1), 1163.
Duffau, H., 2005. Lessons from brain mapping in surgery for low-grade glioma: insights into associations between tumour and brain plasticity. Lancet Neurol. 4 (8), 476–486.
Felleman, D.J., Van Essen, D.C., 1991. Distributed hierarchical processing in the primate cerebral cortex. Cereb. Cortex 1 (1), 1–47.
Setton, R., et al., 2022. Age differences in the functional architecture of the human brain. Cereb. Cortex 33 (1), 114–134.
Guo, T., et al., 2025. Aberrant functional connectome gradient and its neurotransmitter basis in Parkinson's disease. Neurobiol. Dis. 206, 106821.

Zhang, H., et al., 2022. Cortical connectivity gradients and local timescales during cognitive states are modulated by cognitive loads. Brain Struct. Funct. 227 (8), 2701–2712.
Xie, Y., et al., 2024. The efficacy of low frequency repetitive transcial magnetic stimulation for treating auditory verbal hallucinations in schizophrenia: Insights from functional gradient analyses. Heliyon 10 (9), e30194.
Tan, V., et al., 2023. Subgenual cingulate connectivity as a treatment predictor during low-frequency right dorsolateral prefrontal rTMS: a concurrent TMS-fMRI study. Brain Stimul. 16 (4), 1165–1172.
Xie, Y., et al., 2024. Low-frequency rTMS induces modifications in cortical structural connectivity - functional connectivity coupling in schizophrenia patients with auditory verbal hallucinations. Hum. Brain Mapp. 45 (3), e26614.
Blumberger, D.M., et al., 2018. Effectiveness of theta burst versus high-frequency repetitive transcranial magnetic stimulation in patients with depression (THREE-D): a randomised non-inferiority trial. Lancet 391 (10131), 1683–1692.
Lenz, M., et al., 2016. Repetitive magnetic stimulation induces plasticity of inhibitory synapses. Nat. Commun. 7, 10020.
Galanis, C., et al., 2025. Repetitive magnetic stimulation induces plasticity of excitatory synapses through cooperative pre- and postsynaptic activity. Brain Stimul. 18 (5), 1641–1650.
Rao, R.P.N., 2024. A sensory-motor theory of the neocortex. Nat. Neurosci. 27 (7), 1221–1235.
Gorges, M., et al., 2017. Intact sensory-motor network structure and function in far from onset premanifest Huntington's disease. Sci. Rep. 7, 43841.
Samara, A., et al., 2023. Cortical gradients during naturalistic processing are hierarchical and modality-specific. Neuroimage 271, 120023.
Bais, L., et al., 2017. Effects of low frequency rTMS treatment on brain networks for inner speech in patients with schizophrenia and auditory verbal hallucinations. Prog. Neuropsychopharmacol. Biol. Psychiatry 78, 105–113.
Xie, Y., et al., 2023. The Static and dynamic functional connectivity characteristics of the left temporoparietal junction region in schizophrenia patients with auditory verbal hallucinations during low-frequency rTMS treatment. Front. Psych. 14, 1071769.
Vogt;, B.A., 2005. Pain and emotion interactions in subregions of the cingulate gyrus. Nat. Rev. Neurosci. 6 (7), 533–544.
Guo, Z., et al., 2024. Systematic review and meta-analysis: multimodal functional and anatomical neural alterations in autism spectrum disorder. Mol. Autism 15 (1), 16.
Sun, J., et al., 2022. mPFC-rTMS for patients with insomnia disorder using resting-state functional magnetic resonance imaging: a protocol for a randomized controlled trial. Trials 23 (1), 1005.